

Four-Scale Linear Model for Anisotropic Reflectance (FLAIR) for Plant Canopies.

I : Model Description and Partial Validation

H. Peter White^{2,1}, **John R. Miller**², **Jing M. Chen**¹

¹Canadian Centre for Remote Sensing, 588 Booth Street, Ottawa, Ontario, K1A 0Y7, Canada

URL: <http://www.ccrs.nrcan.gc.ca>

²Dept. of Physics and Astronomy, York University, 4700 Keele St., Toronto, Ontario, M3J 1P3, Canada

URL: <http://eol.crestech.ca>

Abstract – As optical remote sensing techniques provide increasingly detailed canopy reflectance data at a variety of illumination/view geometries, direct quantitative comparisons between data sets require a flexible model of the bidirectional reflectance distribution function (BRDF) suitable for inversion. Typically, such derivations rely on: (i) complex and computationally expensive empirical canopy descriptions, or (ii) simplifications for specific canopy types, conditions, or view geometry. More practical would be one general model not requiring significant computing resources, but that provides information on canopy architecture when utilized as an inverse model.

The Four-Scale Model, developed by Chen and Leblanc [1], describes canopy reflectance considering four levels of architecture, distributions of tree crowns, branches, shoots, and leaves. A linear kernel-like model has been developed from this, **FLAIR** (Four-Scale Linear Model for AnIsotropic Reflectance). While simplifications are performed, effort has been made not to limit FLAIR to specific canopy characteristics, while maintaining relationships between modelled coefficients and canopy architecture. Comparisons between Four-Scale and **FLAIR**, and use of **FLAIR** in the forward mode on multi-angular data sets obtained during BOREAS 1994, allow examination of the suitability, capabilities, and limitations of this model in describing canopy reflectance. As partial validation, this paper compares **FLAIR** functions to aspects of the Four-Scale model from which they are developed. Examination of how this model reacts to inversion of simulated reflectance data sets demonstrates its ability to simulate and reproduce canopy reflectance, leading towards the retrieval of reasonable *LAI*. Further validation and examination of this model with field data will be presented in a subsequent paper.

I. INTRODUCTION

Observations continually demonstrate that solar radiance reflected from vegetative canopies can be strongly anisotropic, dependant on the view/illumination geometry. This bidirectional behavior has been extensively investigated; for example see [2], [3], [4], and [5]. This characteristic, as well as variations observed in spatial, temporal, and spectral information, has been utilized as relevant acquired data in platforms such as the U.S. NOAA Advanced Very High Resolution Radiometer (AVHRR), the Advanced Solid-state Array Spectroradiometer (ASAS), the BOREAS-CASI missions, the EOS Multi-angle Imaging Spectro-Radiometer (MISR), Moderate Resolution Imaging Spectrometer (MODIS), and the European Polarization and Directionality of the Earth's Reflectance (POLDER), amongst others.

Effective use of these data sets require reasonable derived reflectance functions. Kernel driven inverse models, describing reflectance as a linear superposition of kernels, provide one way of determining a function from available bidirectional reflectance data, and have been investigated for future sensor validation [6]. Such inverse models use view/illumination geometry and at-surface reflectance to determine a BRDF as well as information on non-angular dependent canopy properties. Many such models exist, some based solely on shape [7] [8], while others are derived from more detailed canopy descriptions [3]. Such semi-empirical models are generally unable to relate coefficients to canopy physical properties. More preferred would be one model that could accurately determine these functions for a variety of canopies, flexible to change in canopy parameters within and between sites, and relates modelled coefficients to canopy physical properties. This has been a goal in recent forward mode models (such as [9]). **FLAIR** development follows this philosophy, derived with specific intent that it not be canopy dependent (beyond the original Four-Scale Model). Partial validation of this model with derived reflectance values from Four-Scale is presented here. Further examination of **FLAIR** with field data will be presented in a subsequent paper.

II. LINEAR MODEL DEVELOPMENT

The Four-Scale Model [1] provides a description of canopy radiative interactions by detailing clumping at the shoot, whorl, branch, and crown architectural levels. Reformulating this model into a linear form that successfully allows inversion would provide a valuable tool towards understanding bidirectional effects on observed reflectance. In so doing, an important aim is to provide a model with sufficient yet minimal number of architectural-based coefficients and angular kernels which allow unique solutions that accurately describe canopy reflectance. Further,

by considering the influence of approximating various Four-Scale Model expressions, derive architectural coefficients that provide quantitative canopy information for a wide range of forest conditions. This would allow the model to provide canopy parameters details for a variety of architectures and would examine view/illumination geometric influences. This methodology is thus unlike some past model developments, where such considerations are either in-part assumed or ranges pre-defined. The FLAIR to Four-Scale validation of approximations used here is carried out making full use of the extensive architectural and reflectance characterizations of boreal forest canopies as measured at BOREAS flux tower sites [10] [11] [12] [13] during the 1994 campaigns, which were also utilized to partially validate the Four-Scale model [1].

Using the Four-Scale terminology (Table 1), linear development of FLAIR is presented as a two-part problem, beginning with two basic probabilities, P_G - the probability of viewing illuminated background, and P_T - the probability of viewing directly illuminated crown foliage. The general form of Four-Scale contains probability coefficients of sunlit ($P_{T,G}$) and shaded ($Z_{T,G}$) overstorey and background with related reflectance factors (R_x) :

$$R = P_T \cdot R_T + Z_T \cdot R_{ZT} + P_G \cdot R_G + Z_G \cdot R_{ZG} \quad (1)$$

Reformulation into a linear form requires isolation of angular from non-angular components for each probability.

A. Probability of Viewing Illuminated Background (P_G)

The background-illuminated proportion defines the probability of observing direct solar-illuminated (not shaded) ground cover. This is expressed in terms of the distribution of gaps in the canopy (canopy gap fraction) allowing both direct viewing through the overstorey (P_{vg}) and directly illuminating the background (P_{ig}), as well as a through-overstorey hot spot function (F_t). When background is viewed through one gap while illuminated through another, the probabilities of viewing and illuminating are not correlated, thus $P_G = P_{ig} \cdot P_{vg}$. When the view line and illumination beam occur via the same gap there is a correlated effect, $P_G = P_{ig}$. The hot spot correlation function provides a normalized description of what contribution each effect has on the overall probability of viewing illuminated background.

$$P_G = P_{ig} P_{vg} + [P_{ig} - P_{ig} P_{vg}] \cdot F_t \quad (2)$$

F_t , the Four-Scale derived hot spot correlation function is a function of the scattering angle (χ) (Equation 3) and the distribution of gap sizes within and between crowns, given by a gap number density $N_t(\mathbf{I})$ which considers both

gaps between trees, determined by the tree density distribution, \mathbf{L} , and gaps through a tree, determined by the leaf density and distribution. As gap sizes increase, there exists a higher probability of viewing direct solar-illuminated background through that gap. This function can be described mathematically for a given canopy type, or can be observed experimentally by an optical instrument. Separation of angular and non-angular components of this function, as described by Four-Scale, proved to be too complex for use in a linear form. An approach was thus adopted to examine the function's shape for a variety of view/illumination angles and canopy gap fractions.

$$\cos(\mathbf{x}) = \cos(\mathbf{q}_i) \cdot \cos(\mathbf{q}_v) + \sin(\mathbf{q}_i) \cdot \sin(\mathbf{q}_v) \cos(\mathbf{f}) \quad (3)$$

The shape of F_t was examined with Four-Scale using architectural parameters as measured at BOREAS (Table 2) for a variety of boreal canopies. In all simulations, $F_t \rightarrow 0$ as the scattering angle becomes large, $\mathbf{x} > 90^\circ$ (forescatter) and also as the view zenith angle approaches a horizontal view perspective, $\mathbf{q}_v \rightarrow 90^\circ$ when $\mathbf{x} < 90^\circ$ (backscatter), indicating that the hot spot region is not symmetric but is more significant on the nadir side, a characteristic observed with other hot spot functions [14]. The computed hot spot is elliptical in shape, with the major axis parallel to the solar plane, matching the hot spot region suggested by multi-angle data sets from many BOREAS sites, such as POLDER [15] or airborne ASAS [16] data. The zenithal width of the hot spot (ZWH) decreases as \mathbf{q}_i increases, due to an increase in the minimum gap size and decrease in the gap frequency. As the hot spot appears to decrease exponentially as \mathbf{x} increases, the following hot spot correlation function is proposed:

$$F = \exp \left(\frac{-2\mathbf{p}\mathbf{x}}{\mathbf{x}_{F \max}} \left[1 - \exp \left\{ \frac{-G(\mathbf{q}) \cdot LAI \cdot \Omega}{\cos(\mathbf{q}_v)} \right\} \right] \right) \quad (4)$$

where:

$$\mathbf{x}_{F \max} = \frac{\frac{1}{2}(\mathbf{p} - \mathbf{q}_i) \left(1 - \left[\frac{\mathbf{q}_i}{\mathbf{p} - \mathbf{q}_i} \right]^2 \right)}{1 + \frac{\mathbf{q}_i}{\mathbf{p} - \mathbf{q}_i} \cos(\mathbf{f}_H)} \quad (5)$$

$$\mathbf{f}_H = \tan^{-1} \left(\frac{\mathbf{q}_v \cdot |\sin(\mathbf{f})|}{\mathbf{q}_v \cdot \cos(\mathbf{f}) - \mathbf{q}_i} \right) \quad (6)$$

With F , the correlation effect is determined relative to the hot spot centre. The term \mathbf{f}_H provides the azimuth angle from the hot spot centre, an angular measure towards \mathbf{q}_v , ranging from 0° to 180° . The term $\mathbf{x}_{F \max}$ defines the

elliptical shape at the full-width half-maximum level, with the hot spot located at one focus of the ellipse, and nadir located on the perimeter on the major axis opposite of the ellipse's centre. This sets the semi-major axis (one half ZWH) as $((\mathbf{p}\cdot\mathbf{q}_i)/2)$ and the eccentricity as $(\mathbf{q}_i/(\mathbf{p}\cdot\mathbf{q}_i))$.

This description incorporates some basic implicit structural information about the canopy, and has not been completely separated into angular and non-angular terms. Such a form lacks any implicit structural information about crown spacing or distribution within the forest site. This results in a relatively less steep hot spot function compared to that determined by Four-Scale which directly models foliage clumping into distinct crowns, decreasing the probability of through-crown and within-crown correlated view and illumination proportions. The proposed function is demonstrated (Figure 1) for tall trees with high LAI (Old Black Spruce) and short trees with low LAI (Young Jack Pine). While discrepancies exist with respect to the more complex Four-Scale derivation, these deviations are within the realm of other hot spot functions, such as those examined by Qin and Goel [14].

The individual probabilities of having illuminated background (P_{ig}) or viewed background (P_{vg}) are determined geometrically. Four-Scale examines how gaps within and between crowns contribute to a solar beam penetrating unscattered to reach the background. The calculation incorporates the crown's effective LAI, L_e , projected perpendicular to the view/illumination direction, the tree distribution, and the potential of the view/illumination beam passing through multiple crowns without scattering. As this calculation did not lend itself to be expressed in a basic linear form, an equation for the gap probability for a discontinuous canopy, similar in form to that described by Li and Strahler [17], but modified to include the effect of foliage clumping within the canopy, is used:

$$P_{(i,v)g}(\mathbf{q}_{(i,v)}) = \exp\left(\frac{-G(\mathbf{q}) \cdot LAI \cdot \Omega}{\cos(\mathbf{q}_{(i,v)})}\right) \quad (7)$$

where LAI is the mean canopy overstorey leaf area index and \mathbf{W} is the canopy clumping index (nonrandomness factor) described in [1] and [10].

This function (Equation 7), compared to the more complex Four-Scale form, is similar in shape and magnitude when determined for forests with low foliage crown density (YJP simulations, Figure 2). However, when the within crown foliage becomes tightly clumped, Four-Scale determines a more linear P_{vg} , especially as tree crown density increases (see the OBS simulations). With Four-Scale, the intensity of this peak is partly related to a geometric tree description which contains strict outer crown surface boundaries. More realistically, tree crown edges are jagged,

not conforming to a “cone on a cylinder” shape, but with branches and gaps occurring at the outer crown surface. Further study is required to examine the applicability of using a strict geometric shape where highly clumped crown foliage is concerned, however in the FLAIR model application, no perimeter shape parameterization is required.

In general use, the probability of viewing directly solar-illuminated background may be expressed as:

$$P_G = P_{ig} [F(1 - P_{vg}) + P_{vg}] \quad (8)$$

In cases of more moderate LAI values (between 1 and 4) commonly seen in boreal forests [15] [10] [18], this form of P_G provides reasonable values compared to those determined by Four-Scale (Figure 3). For more extreme cases of dense vegetation, FLAIR modelled P_G reproduces the general shape and magnitude relative to those calculated by Four-Scale, with a distinct difference occurring near nadir. This discrepancy decreases as tree density or LAI decreases, and is again due to Four-Scale using a rigid geometrical shape to describe the tree crown.

B. Probability of Viewing Illuminated Crown Foliage (P_T)

As with P_G , the probability of viewing illuminated crown foliage is subject to correlated and non-correlated effects. When within-crown foliage is viewed through the same gap as the direct incident solar illumination, the probability of viewing illuminated foliage is one minus the probability of illuminating the background, $(1 - P_{ig})$. When illumination occurs through a different gap, then one must define the probability of viewing that foliage within the crown (P_{Tf}), as well as the probability of viewing a crown $(1 - P_{vg})$. A within-canopy hot spot function, $F_s(\mathbf{x})$, is used in Four-Scale to define correlated and non-correlated influences, based on within-crown gaps:

$$P_T = P_{Tf} (1 - P_{vg}) + [(1 - P_{ig}) - P_{Tf} (1 - P_{vg})] \cdot F_s \quad (9)$$

Examination of F_s demonstrates that it shares many common traits with F_t (Figure 1). Direct comparison of these functions demonstrates a satisfactory agreement with each other; as the leaf density decreases, the hot spot function gradient decreases. Thus the hot spot correlation function is treated as equivalent, allowing $F_s(\mathbf{x}) = F_t(\mathbf{x}) = F(\mathbf{x})$.

The probability P_{Tf} includes the contributions of sunlit foliage within the sunlit crown proportion (Q_1) and sunlit foliage within the self-shaded parts of the crown (Q_2). Here, shaded and sunlit crown portions are determined geometrically as a solid-surfaced crown (P_{ii}), providing the Four-Scale derived relationship for the probability of viewing illuminated foliage as:

$$P_{Tf} = P_{ii} \cdot Q_1 + (1 - P_{ii}) \cdot Q_2 \quad (10)$$

The sunlit foliage component expressions were examined. When $\mathbf{q}_i \rightarrow 0^\circ$, the proportion of viewed crown that is illuminated remains high for the entire backscatter region, and the contribution of $(1 - P_{ii}) \cdot Q_2$ is minor compared to $P_{ii} \cdot Q_1$. Also, with decreasing LAI , Q_2 values approach Q_1 . This is also observed when $\mathbf{q}_i \rightarrow 90^\circ$, as sunlit and shaded proportion values are again similar (i.e. $Q_1 \approx Q_2$). Such canopy conditions would allow the northern “predominately shaded” side of a crown to have foliage exposed to sunlight at some significant level.

Using $Q_1 \approx Q_2$ greatly simplifies reformulating Four-Scale, as the sunlit and shaded proportions of viewed crown are no longer needed (P_{ii} no longer has to be determined). Thus the function P_{Tf} can be approximated using Q_1 .

$$\begin{aligned} P_{Tf} &\approx P_{ii} \cdot Q_1 + (1 - P_{ii}) \cdot Q_1 \\ P_{Tf} &\approx Q_1 = \Gamma(\mathbf{x}) \cdot \left[1 - e^{-L_H(C_i + C_v)} \right] \cdot \left[\frac{C_i C_v}{C_i + C_v} \right] \end{aligned} \quad (11)$$

Further, the exponential expression of this function can be approximated as $\left[1 - e^{-L_H(C_i + C_v)} \right] \approx 1$ (using $L_H(C_i + C_v) \gg 1$, especially true for large leaf densities [20]). This provides a simpler approximating function:

$$P_{Tf} \approx \Gamma(\mathbf{x}) \left(\frac{C_i C_v}{C_i + C_v} \right) \quad (12)$$

where:

$$C_{i,v} = \frac{G(\mathbf{q}_{i,v})}{\sin(\mathbf{q}_{i,v} + \mathbf{a}_{cone})} \cdot \Omega \quad (13)$$

and \mathbf{a}_{cone} is defined as the half apex angle of the conical crown top. As tree crowns do not follow strict geometric structures, a mean value of $\mathbf{a}_{cone} = 15^\circ$ is used as representative. The probability of viewing within-crown solar-illuminated foliage can now be expressed as:

$$P_{Tf} = \Omega \cdot \Gamma(\mathbf{x}) \left(\frac{G(\mathbf{q})}{\sin(\mathbf{q}_i + 15^\circ) + \sin(\mathbf{q}_v + 15^\circ)} \right) \quad (14)$$

where a first-order geometric scattering phase function is provided by Chen and Leblanc [1]:

$$\Gamma(\mathbf{x}) = \left(1 - \frac{C_p \mathbf{x}}{\mathbf{p}}\right), \quad C_p = 0.75 \quad (15)$$

In Four-Scale an asymmetry factor is determined assuming a value that best fits a theoretical description of the foliage environment. If foliage elements were solid isotropic spheres C_p would be unity. More porous, less spherical elements have smaller values, leading to Chen and Leblanc's choice of 0.75 as applicable to a forest canopy.

Further considerations to P_{Tf} are the components related to needle and shoot distributions. Examination of W reveals that the nonrandomness factor [10] [19] for boreal conifer species is observed to range around 0.5. For the sample boreal deciduous species (old aspen site), where individual leaves are not distributed in shoots, this value approaches unity. Thus this value, for this expression only, may be treated as known instead of variable, which results in P_{Tf} being approximated by an angular expression, with a set structural coefficient (0.5 for conifer, 0.75 for mixed or unknown, and 1 for deciduous).

The probability of viewing sunlit crown elements may now be expressed as:

$$P_T = F \cdot (1 - P_{ig}) + (1 - F) \cdot P_{Tf} \cdot (1 - P_{vg}) \quad (16)$$

As verification, values of P_T were calculated and compared to those determined by Four-Scale. In all cases, the general shape and magnitude of the Four-Scale calculation was reproduced. In short, thin crown simulations, (YJP, Figure 4), similar results are observed for high tree densities, with slightly lower values for low tree densities determined by Equation 16. At the other extreme, with slender tall, thick crowns (OBS), the opposite is observed.

C. Probability of Viewing Shaded Components (Z_T and Z_G)

These shaded canopy proportions define viewed canopy areas not directly solar-illuminated, receiving radiation only from diffuse sky and canopy multiple scattering. The probability of viewing shaded overstorey (Z_T) is simply that fraction of the scene where background or directly illuminated overstorey is not viewed :

$$Z_T = 1 - P_{vg} - P_T \quad (17)$$

Similarly, the probability of viewing shaded background, Z_G , is that part of the scene where overstorey or directly illuminated background is not viewed :

$$Z_G = P_{vg} - P_G \quad (18)$$

In sample simulations, these modelled shaded proportions reasonably reproduced those determined with the Four-Scale Model, with an over-estimation sometimes occurring near nadir in cases of dense forests with thick crowns.

In all Four-Scale derived probabilities a nadir discontinuity often appears. This is caused in part by the increased presence of viewed background at nadir, but more significantly by the change in the horizontally-projected tree geometry that occurs as the conical top no longer becomes part of the projected shadow (at $q=a$). This is most apparent in cases of dense within-crown foliage. Chen and Leblanc [1] recognized this, describing the modelled crown as "simplified geometry", referring to a tree crown not having a definite confined regular geometric shape, but instead having edge gaps and branch projections. In contrast, reference to crown shape in this derivation comes from describing how scattering within and between crowns may occur, leaving to the investigator the subsequent task of relating the derived canopy *LAI* to the tree crown structural parameters.

D. Canopy Multiple Scattering

While defining the proportions of shaded overstorey and background provides an important aspect towards understanding and modelling canopy reflectance, use of such proportions requires information on how being in "shade" affects the observed reflected radiative flux. The Four-Scale Model applies a factor to the "directly sunlit" reflectance factors to describe this influence as a shaded reflectance factor, with the expressions:

$$\frac{R_{ZT}}{R_T} = C_m \cdot F_{dt} \quad (19)$$

$$\frac{R_{ZG}}{R_G} = C_m \cdot F_{dg} \quad (20)$$

More investigation is required to better understand the fraction of downwelling irradiance due to canopy multiple scattering (C_m), as well as the fraction due to diffuse sky irradiance near the top (F_{dt}) and bottom of the stand (F_{dg}) in order to determine the average shaded crown reflectance factor (R_{ZT}) and shaded background reflectance factor (R_{ZG}). Recognizing that the shaded-to-sunlit reflectance factor ratio is not zero allows for contributions of shaded components to the observed reflectance to be approximated. As a lack of data exists to model these fractions, the ratio of shaded-to-sunlit reflectance factors are treated individually, with first order approximations referred to here as multi-scattering factors, with wavelength-dependent values applicable to the overstorey and background.

A first-order estimate of the background multi-scattering factors for the BOREAS sites were examined using the ratio of observed ground target nadir radiance in shade to a standard panel nadir radiance in direct sunlight [20].

This examination loosely suggests that an angularly constant, wavelength dependent value may be appropriate during summer months. This is consistent with a recent theoretical examination of shaded background component reflectance factors used in the GORT Model [9]. Observational uncertainties in defining background regions as purely shaded or completely sunlit prevent a definite analysis. There is indication of a wavelength dependence in winter, when the Sun is near the horizon, with an increase in scattered light occurring towards shorter wavelengths. Here the multi-scattering factors will be treated as angularly-independent wavelength dependent constants.

III. FLAIR MODEL FORMULATION

Using the above descriptions, canopy BRDF may be determined using a linear kernel model-like form, derived as:

$$R = R_T P_T + R_G P_G + R_{ZT} (1 - P_{vg} - P_T) + R_{ZG} (P_{vg} - P_G) \quad (21)$$

After substitution for the probabilities discussed above, this may be re-written into a four coefficient expression :

Full Model:	Full Model (Kernel Form):
$R = R_{zt} \times \left[(1 - P_{vg}) - F(1 - P_{ig}) - P_{Tf}(1 - F)(1 - P_{vg}) \right]$	$R = R_{zt} \times k_1$ (22)
$+ R_{zg} \times \left[P_{vg} - P_{ig} \{ F(1 - P_{vg}) + P_{vg} \} \right]$	$+ R_{zg} \times k_2$ (23)
$+ R_t \times \left[F(1 - P_{ig}) + P_{Tf}(1 - F)(1 - P_{vg}) \right]$	$+ R_t \times k_3$ (24)
$+ R_g \times \left[P_{ig} \{ F(1 - P_{vg}) + P_{vg} \} \right]$	$+ R_g \times k_4$ (25)

As a linear kernel model, FLAIR does not completely succeed in separating angular from non-angular contributions. While coefficients are defined based on the four reflectance factors, the kernels ($k_{1,2,3,4}$) contain the terms $G(\mathbf{q}) \cdot LAI \cdot \Omega$. As discussed above, \mathbf{W} may be approximated by 0.5 for conifer, 0.75 for mixed canopies, and unity for deciduous. The unit leaf area projection is commonly modelled by the random case, $G(\mathbf{q}) = 0.5$ [1][3][20]. This leaves canopy LAI as a non-angular unknown kernel term. This factor is determined by running the inverse model over multiple LAI values, and determining the best result, as described in the next section.

IV. FLAIR FORWARD AND INVERSE ALGORITHM DEVELOPMENT

As developed, the **Four-Scale Linear Model for An Isotropic Canopy Reflectance (FLAIR)** provides the potential to compare canopy BRF of temporal or spatially distinct data sets. The impact of each kernel on derived coefficients depend on the bidirectional geometry. Angular kernel functions are demonstrated for three values of \mathbf{q} ; (Figures 5) for a LAI of 2. Note regions where kernels approach zero, or have similar shapes and magnitudes. Limiting bidirectional angular sampling to these regions could produce unrealistic coefficient retrievals. Thus a wide range of view/illumination angles have the potential of providing better results.

The initial inverse **FLAIR** algorithm was designed using a straight forward matrix inversion to determine the four reflectance factors for a given LAI . This was found sufficient for a large number of observations, but when a small number ($N < 10$) was used non-realistic and multiple solutions resulted. This is due in part to observational accuracy in measuring (or calculating) reflectance and in recording the angular geometry of the sensor and Sun. Inverse derived coefficients were found to be sensitive to small error in observed reflectance, especially when a limited range of observing geometry was used (such as one illumination angle and near nadir only views) [20]. A method limiting the derived reflectance factors to more realistic solutions was thus required.

The inverse FLAIR algorithm is based on a modified simplex method [21]. Normally, a simplex algorithm works by setting constraints to a set of independent variables and determining a maximum value of a function passing within these boundaries (optimal feasible vector). Two adjustments to this method were adopted.

In defining primary reflectance factor constraints, one may simply note the expected range, namely:

$$R_{zt} \geq 0 ; R_{zg} \geq 0 ; R_t \geq 0 ; R_g \geq 0 \quad (26)$$

$$R_{zt} \leq R_t ; R_{zg} \leq R_g ; R_t \leq 1 ; R_g \leq 1 \quad (27)$$

Additional constraints come from the observations. Using each observation as an individual constraint can result in a time consuming procedure involving the use of potentially redundant or non-compliant information. To avoid this, the additional constraints were defined based on a technique described in [22], where given N observed reflectance values, four linear equations are defined :

$$\begin{aligned} \sum_{j=1}^N (BRF_j k_{ji}) = R_{zt} \sum_{j=1}^N (k_{ji} k_{j1}) + R_{zg} \sum_{j=1}^N (k_{ji} k_{j2}) \\ + R_t \sum_{j=1}^N (k_{ji} k_{j3}) + R_g \sum_{j=1}^N (k_{ji} k_{j4}) \end{aligned} ; i = 1,2,3,4 \quad (28)$$

where: k_{ji} is kernel number i calculated for observation j , and BRF_j is the reflectance for observation j .

Recall however that these kernels contain within them canopy *LAI*. Also, observational errors and experimental accuracy related to sensor field-of-view, instrument calibration and positioning, and atmospheric correction exists. If no errors in observation or approximations in the modelled canopy description existed, then one could simply invert the model equations to determine reflectance factors. As this is not the case, a discrepancy factor, f , is introduced to provide eight equations that are used as additional constraints to the model.

$$\begin{aligned} \sum_{j=1}^N (f \cdot BRF_j k_{ji}) \geq R_{zt} \sum_{j=1}^N (k_{ji} k_{j1}) + R_{zg} \sum_{j=1}^N (k_{ji} k_{j2}) \\ + R_t \sum_{j=1}^N (k_{ji} k_{j3}) + R_g \sum_{j=1}^N (k_{ji} k_{j4}) \end{aligned} ; i = 1,2,3,4 \quad (29)$$

$$\begin{aligned} \sum_{j=1}^N (f^{-1} \cdot BRF_j k_{ji}) \leq R_{zt} \sum_{j=1}^N (k_{ji} k_{j1}) + R_{zg} \sum_{j=1}^N (k_{ji} k_{j2}) \\ + R_t \sum_{j=1}^N (k_{ji} k_{j3}) + R_g \sum_{j=1}^N (k_{ji} k_{j4}) \end{aligned} ; i = 1,2,3,4 \quad (30)$$

Equations 29 and 30 define hyperplanes in the 4-D virtual-space of component reflectance factors. An optimal feasible vector is defined to go through this region. For FLAIR inversion, the function used is the BRF for nadir view and -45° illumination, $BRF(0^\circ, 45^\circ, 180^\circ)$, chosen as a potential view/illumination orientation that could act as a convenient normalization standard that would not be adversely affected by errors that might be introduced by the steep gradient in the area of the hot spot.

A poor choice of f , if too large, results in the hyperplanes not intersecting within the area defined by the primary constraints, resulting in derived reflectance values of 1 and 0. If f is too small, then the hyperplanes define no bound regions within which to pass a feasible vector. Thus, inversion is initially performed for large f , and is decreased using a bisection algorithm, minimizing the size of the bound region to an infinitesimally small (within

computational error) area containing the optimal feasible vector. This results in the area converging on the derived values of the four component reflectance factors.

Inversion is performed for various LAI values. The derived LAI and component reflectance factors are then used by FLAIR in the forward mode to reproduce the initial BRF's. Relative errors between reflectance calculated from the inverted functions (\mathbf{r}_i) and those simulated with Four-Scale (\mathbf{r}_f) are examined by determining both a correlation coefficient (Equation 31) and a root mean square error ($RMSE$) (Equation 32) to meet model validation conditions as outlined in previous studies [22] [23].

$$r_{cc} = \frac{\sum(\mathbf{r}_{i_i} - \overline{\mathbf{r}_i})(\mathbf{r}_{f_i} - \overline{\mathbf{r}_f})}{\left[\sum(\mathbf{r}_{i_i} - \overline{\mathbf{r}_i})^2 \sum(\mathbf{r}_{f_i} - \overline{\mathbf{r}_f})^2 \right]^{1/2}} \quad (31)$$

$$RMSE = \left\{ \frac{1}{(N-n)} \sum_{i=1}^N (\mathbf{r}_{i_i} - \mathbf{r}_{f_i})^2 \right\}^{1/2} \quad (32)$$

The optimal LAI for inversion is determined by identifying that value which produces a high r_{cc} and low $RMSE$. A further constraint is imposed, if a small change in LAI results in a large change in reflectance factor values, the result is assigned a large error. This assumes that if the model is converging with a realistic LAI , small changes in LAI would result in small, not large, changes in derived reflectance factors. This was found necessary to prevent near zero or near infinity LAI values from dominating every solution.

V. FLAIR VALIDATION

A. Validation Relative to Four-Scale Model Produced BRF Values

While **FLAIR** provides a mathematical formulation generally consistent with the Four-Scale Model, the ability to derive representative canopy BRF's needs demonstration. During derivation, individual expressions used by FLAIR were compared to equivalent Four-Scale expressions. Validation can also be performed in part by determining and comparing reflectance simulated with Four-Scale and forward mode FLAIR, using identical input parameters.

The Four-Scale Model was used to determine BRF values at 5^0 view angle intervals in the solar plane and at 30^0 view angle intervals in the cross-solar plane and at 45^0 to the solar plane using the nominal summer OBS, YJP and OJP architectural values (Table 2), with \mathbf{q}_i ranging from 15^0 to 75^0 at 30^0 intervals (Figure 6). BRF values were then

derived for the same orientations using forward mode FLAIR (f-FLAIR). The results were compared with r_{cc} and $RMSE$ determined between each unique \mathbf{q}_i pair of calculated data sets (Table 3).

For large tree crown density, high LAI conditions observed at the southern OBS sites [15], f-FLAIR produces canopy BRF that reproduce the general shape and magnitude of the Four-Scale data sets, with a wider apparent hot spot effect (Figure 7) in the foreshadow direction. Comparing BRF values derived with the high tree density, low LAI conditions (YJP sites) demonstrated a high correlation between Four-Scale and FLAIR. When a similar comparison is performed on low LAI , low tree density simulations (OJP sites), FLAIR modelled BRF values were found to match or be slightly higher magnitude than those determined by the Four-Scale Model.

VI. INVERTING FLAIR - FURTHER VALIDATION

A. Inverting to Produce a Function for Canopy BRF

One purpose towards the development of FLAIR is to be able to utilize the model in the inverse mode. To this end, FLAIR was further validated by inverting a subset of angularly-sampled BRF values produced by simulations with the Four-Scale Model.

BRF values from each Four-Scale simulation were determined at view angles at 15° intervals along the solar plane (from -60° to $+60^\circ$), and at 30° intervals off-solar plane, for a total of eleven data points. Each unique illumination angle data subset (uni- \mathbf{q}_i) was then used to derive canopy BRF for each of $\mathbf{q}_i = -15^\circ, -45^\circ, -75^\circ$ based on the inverse FLAIR algorithm (i-FLAIR). The derived functions were then used to re-determine BRF values for all \mathbf{q}_i initially used to produce the simulated data, and were then compared to the initial Four-Scale derived data sets. The uni- \mathbf{q}_i subsets were then combined to produce a multiple illumination angle set (multi- \mathbf{q}_i) and i-FLAIR derived BRF was again used to reproduce the Four-Scale Model simulated data.

For all summer simulations, i-FLAIR functions were found to reproduce the simulated BRF curves and locate the hot spot. i-FLAIR functions generally produced reflectance of a slightly lower magnitude around the hot spot region, demonstrated with the summer and winter OBS $\mathbf{q}_i=-45^\circ$ simulations (Figure 8). $RMSE$ and r_{cc} for all summer simulations are provided in Table 3.

As recent research has begun to note the significance of the background on canopy reflectance [24], winter simulations (using Table 2 properties with $R_g=R_G=0.85$ [20]) were examined. i-FLAIR derived functions were able to reproduce Four-Scale simulated BRF and the hot spot location. While i-FLAIR functions reproduced the data sets

with high r_{cc} and low $RMSE$, the nadir reflectance was often noticeably shifted relative to the Four-Scale simulated data for large LAI and q_i . This occurs due to the previously discussed Four-Scale geometric crown description.

B. Inverting to Determine Architectural Coefficients

As discussed, FLAIR coefficients may be determined in the forward mode using measured canopy architectural values and reflectance factors and by estimating the shaded-to-sunlit reflectance factor ratios (multi-scattering factors) for both the overstorey and background. By inverting the Four-Scale simulated data sets, i-FLAIR derived coefficients may be compared to their forward calculated values to assess the potential of relating inverted coefficients to the canopy parameters.

Using these simulations, comparisons between forward mode and inverse mode FLAIR may be performed. The five near infrared canopy parameters from the three summer simulations are presented in Figure 9 (summer and winter simulations in the red band produced similar results). In these models, LAI was determined independent of wavelength. Further work with FLAIR will examine setting LAI to be constant across multiple wavelength bands.

Comparison between measured canopy parameters [1] and i-FLAIR parameters demonstrate a good correlation, especially in old and young jack pine simulations where crown geometric structure is not as significant. In the densely packed OBS crowns, i-FLAIR derived LAI and crown reflectance factors were less than those used to produce the Four-Scale simulations. This is due in part to the FLAIR approximation used for the probability of viewing/illuminating the background through the overstorey (Equation 6) being more significantly different than that used by the Four-Scale Model, discussed in the preceding section. Also relevant here, the nonrandomness factor is assumed 0.5 for all conifer canopies. The tighter foliage clumping in black spruce canopies may be better modelled by a more complex nonrandomness expression [10], however more research is required. By using a more homogeneous foliage distribution in the overstorey, i-FLAIR results in an under-estimation of LAI and overstorey reflectance factors relative to the Four-Scale Model. With jack pine simulations, where tree size and distributions naturally result in a more homogeneous foliage distribution, i-FLAIR was better able to reproduce the initial canopy parameters used by Four-Scale to produce the canopy simulations. When comparing overstorey LAI determined for each wavelength band, inverse derived values were similar for all simulations. Such a result supports treating overstorey LAI as a wavelength independent parameter in future inverse FLAIR algorithms. Canopy parameters used to produce Four-Scale canopy simulations and parameters derived by multi- q_i FLAIR inversion of the simulated BRF's are provided in Table 4.

VII. CONCLUSIONS AND FURTHER WORK

In this paper, a linear derivation of the Four-Scale Model is presented. The **FLAIR** model is derived following specific goals not generally applied to linear kernel model development. Namely these are: 1) maintain general applicability to a wide range of canopy architectural and optical properties; 2) develop coefficients that maintain a relationship with canopy properties; and 3) provide a model that works equally well in forward and inverse modes. In following these goals, a pre-defined number of kernels was not set; instead the linearization procedure resulted in a four kernel, five parameter model. The coefficients are related to the four optical canopy properties (R_G , R_T , R_{ZG} , and R_{ZT}) and one structural property, overstorey LAI . By following this derivation technique, one starts to examine which properties are directly obtainable from remote observation, instead of attempting to bias the answer by pre-defining which canopy architectural or optical properties to retrieve. In FLAIR, a bias is made towards more homogeneous foliage distributions, but the model design does not limit its use to such canopies.

A partial validation of FLAIR has been demonstrated with respect to the Four-Scale Model in two ways. First, both models were used to simulate canopy BRF using the same architectural and reflectance properties. f-FLAIR modelled canopy BRF reproduced that determined by Four-Scale for all test cases. Second, i-FLAIR was used to invert a subset of Four-Scale simulated BRF's. Each canopy simulation was successfully inverted by FLAIR to produce a function that could be used to reproduce the complete Four-Scale canopy simulated data sets, both summer and winter. i-FLAIR functions were also found to produce realistic canopy parameters, comparable to the values used in calculating the Four-Scale canopy simulations.

The next important stage in FLAIR validation will be to examine field data. This will be done in part with data obtained as part of BOREAS 1994, using architectural and optical properties measured in-field, as well as multi-angle canopy bidirectional reflectance values obtained with a variety of sensors, such as the multi-season, bidirectional CASI data sets [20][24][25]. Other BOREAS data sets (such as with POLDER) will provide additional information towards validation and use of the FLAIR model. The aim will be to compare i-FLAIR results to seasonal change within a specific canopy, as well as to examine differences between species type.

AKNOWLEDGEMENT

We would like to thank S. Leblanc who provided valuable comments during the derivation of FLAIR, and the anonymous reviewers who provided thorough and helpful reviews of this manuscript.

REFERENCES

- [1] J. M. Chen and S. G. Leblanc, "A four-scale bidirectional reflectance model based on canopy architecture", *IEEE Trans. GeoSci. Remote Sens.*, vol. 35, No. 5, pp. 1316-1337, 1997.
- [2] J. Cihlar, D. Manak, and N. Voisin, "AVHRR bidirectional reflectance effect and compositing", *Remote. Sens. Environ.*, vol. 48, pp. 77-88, 1994.
- [3] W. Wanner, X. Li, and A. H. Strahler, "On the derivation of kernels for kernel-driven models of bidirectional reflectance", *J. Geophys. Res.*, vol. 100 (D10), pp. 21077-21089, 1995.
- [4] A. Wu, Z. Li, and J. Cihlar, "Effect of land cover type and greenness on advanced very high resolution radiometer reflectance: analysis and removal", *J. GeoPhys. Res.*, vol. 100 (D10), pp. 9179-9192, 1995.
- [5] H. P. White, J. R. Miller, J. M. Chen, and D. R. Peddle, "Seasonal change in mean understory reflectance for BOREAS sites: Preliminary results", in *Proc. 17th Can. Symposium on Remote Sensing*, pp. 189-194, 1995.
- [6] B. Hu, W. Lucht, X. Li, and A. Strahler, "Validation of kernel-driven semiempirical models for the surface bidirectional reflectance distribution function of land surfaces", *Remote Sens. Envir.*, v.62, pp. 201-214, 1997.
- [7] C. L. Walthall, J. M. Norman, J. M. Welles, G. Campbell, and B. L. Blad, "Simple equation to approximate the bidirectional reflectance from vegetation canopies and bare soil surfaces", *Appl. Opt.*, v.24, pp. 383-387, 1985.
- [8] H. Rahman, B. Pinty, and M. M. Verstraete, "Coupled Surface-Atmosphere Reflectance (CSAR) model. 2. Semiempirical surface model usable with NOAA Advanced Very High Resolution Radiometer data", *J. Geophys. R.*, vol. 98 (D11), pp. 20791-20801, 1993.
- [9] W. Ni, X. Li, C. E. Woodcock, M. R. Caetano, and A. H. Strahler, "An analytical hybrid GORT model for bidirectional reflectance over discontinuous plant canopies", *IEEE Trans. GeoSci. Remote Sens.*, vol. 37 (2), pp. 987-999, 1999.
- [10] J. M. Chen, "Optically-based methods for measuring seasonal variations of leaf area index in boreal conifer stands", *Agric. For. Meteorol.*, vol. 80, pp. 138-163, 1996.
- [11] R. Soffer, *Bidirectional Reflectance Factors of an Open Tree Canopy by Laboratory Simulation*, MSc. Thesis, Graduate Programme in Earth and Space Science, York University, Ontario, 1995.

- [12] H. P. White, J. R. Miller, R. Soffer, and W. Wanner, "Semiempirical modelling of bidirectional reflectance utilizing the MODIS BRDF/Albedo algorithm models", *Proc. IGARSS'96*, 1996.
- [13] E. M. Middleton, E. A. Walter-Shea, M. A. Mesarch, S. S. Chan, and R. J. Rusin, "Optical properties of canopy elements in black spruce, jack pine, and aspen stands in Saskatchewan, Canada.", *Can. J. Remote Sens.*, vol. 23., pp. 188-199, 1996.
- [14] W. Qin, and N. S. Goel, "An evaluation of hot spot models for vegetation canopies", *Remote Sens. Reviews*, vol. 13., pp.1-2, 1995.
- [15] S. G. Leblanc, P. Bicheron, J. M. Chen, M. Leroy, and J. Cihlar, "Investigation of radiative transfer in boreal forests with an improved 4-scale model and airborne POLDER data", *IEEE Trans. Geosci. Remote Sens.*, vol. 37, pp. 1396-1414, 1997.
- [16] C. A. Russell, J. R. Irons, and P. W. Dabney, "Bidirectional reflectance of selected BOREAS sites from multiangle airborne data", *J. Geophys. R.*, vol. 102 (D24), pp. 29505-29516, 1997.
- [17] X. Li and A. H. Strahler, "Modeling the gap probability of a discontinuous vegetation canopy", *IEEE Trans. Geosci. Remote Sensing*, vol. 26, pp. 161-169, 1988.
- [18] S. E. Loechel, C. L. Walthall, E. B. de Colstoun, J. M. Chen, and B. L. Markham, "Spatial and temporal variability of surface cover at BOREAS using reflectance from a helicopter platform", *IEEE Trans. Geosci. Remote Sens.*, vol. 34, pp. 586-590, 1996.
- [19] C. J. Kucharik, J. M. Norman, L. M. Murdock, and S. T. Gower, "Characterizing canopy nonrandomness with a multiband vegetation imager (MVI)", *J. Geophys. R.*, vol. 102 (D24), pp. 29409, 1997.
- [20] H. Peter White, *Investigations of Boreal Forest Bidirectional Reflectance Factor (BRF)*, Ph.D. Thesis, Graduate Programme in Physics and Astronomy, York University, Ontario., 1999.
- [21] W. T. Vetterling, S. A. Teukolsky, W. H. Press, and B. P. Flannery, *Linear Programming and the Simplex Method*, Numerical Recipes in C, Press Syndicate of the University of Cambridge, Cambridge UK., 1990.
- [22] A. H. Strahler, and J. Muller, "MODIS BRDF/Albedo product: algorithm theoretical basis document", version 3.2, NASA EOS MODIS, 1995.

- [23] N. S. Goel, "Inversion of Canopy Reflectance Models for Estimation of Biophysical Parameters From Reflectance Data", in *Theory and Applications of Optical Remote Sensing.*, G. Asrar, ed., John Wiley and Sons, New York, pp.205-251, 1998.
- [24] B. Hu, K. Inanen, J. Miller, "Retrieval of Leaf Area Index and Canopy Closure from CASI Data over the BOREAS Flux Tower Sites", submitted to *Remote Sensing of Environ.*, July 1999.
- [25] J. R. Miller, J. Freemantle, P. Shepherd, L. Gray, N. O'Neill, A. Royer, and E. Senese, "Development of CASI to meet the needs of BOREAS science", *Proc. 17th Can. Symp. Remote Sensing*, Saskaton, SK, 1995.

LIST OF FIGURES

Figure 1 : Comparison of Four-Scale derived hot spot functions and the FLAIR hot spot function for various tree densities of a) young jack pine and b) old black spruce. Solar illumination angle is indicated with a gray dot.

Figure 2 : Comparison of Four-Scale derived and a cosine based derived probability of viewing background (P_{vg}) for young jack pine and old black spruce for 1000trees/ha, and 4000trees/ha.

Figure 3 : Comparison of Four-Scale and FLAIR derived probability of viewing illuminated ground cover (P_G) for old black spruce and young jack pine simulations.

Figure 4 : Comparison of Four-Scale and FLAIR derived probability of viewing illuminated tree crown (P_T) for old black spruce and young jack pine simulations.

Figure 5 : Solar plane derived values for FLAIR modelled inverse kernels for $LAI=2$ and solar illumination zenith angles of a) nadir, b) -30^0 , and c) -60^0 .

Figure 6 : View locations of Four-Scale derived BRF values. Azimuth angles are provided outside the perimeter. The Sun is located at an azimuth of 180^0 (south), at various zenith angles. Due to azimuthal symmetry, BRF values at view azimuth angles between 0^0 and 180^0 only (east) are processed.

Figure 7 : Solar plane BRF values calculated with the Four-Scale Model and FLAIR (in the forward mode) for a) OBS and b) OJP.

Figure 8 : Solar plane BRF values calculated with the Four-Scale Model and inverted FLAIR functions for OBS summer and winter simulations. Note the nadir peak produced by the Four-Scale Model.

Figure 9 : Summer OBS near infrared simulations. Derived coefficients using the FLAIR model in the forward mode, and in the inverse mode using the complete multi- \mathbf{q}_i data sets, and data sets at unique \mathbf{q}_i values.

LIST OF TABLES

Table 1: Symbol nomenclature used in this paper.

Table 2: Input model data from observed field data for BOREAS'94 Tower Flux sites.

Table 3: Correlation coefficients and RMSE between Four-Scale Model derived BRF values and forward mode FLAIR derived BRF values using the same field data, and inverted FLAIR derived functions based on the Four-Scale values

Table 4: Red and near infrared canopy parameters as determined from derived inverse FLAIR calculations based on Four-Scale forward calculated BRF values. (Simulation in the red wavelength region produced similar comparisons between the two models and thus are not shown here.)

\mathbf{a}_{cone}	The half apex angle of the conical top of a modelled tree crown.
$BRDF$	Bidirectional Reflectance Distribution Function
BRF	Bidirectional Reflectance Factor
C_m	Fraction of downwelling irradiance due to multiple scattering within the canopy.
C_p	Foliage asymmetry factor.
F	Hot spot correlation function.
F_{dt}, F_{dg}	Fraction of downwelling irradiance due to diffuse sky irradiance as viewed near the top of the canopy and near the bottom of the canopy respectively.
\mathbf{g}_E	Needle-to-shoot ratio
$\mathbf{G}(\mathbf{x})$	First-order scattering (geometric shadow) phase function of a foliage element.
$G(\mathbf{q})$	Projection of unit leaf area.
\mathbf{f}_i	Solar Illumination Azimuth Angle.
\mathbf{q}_i	Solar Illumination Zenith Angle.
k_i	FLAIR kernel designation.
LAI	Leaf Area Index
\mathbf{W}_E	Clumping index of the crown element
\mathbf{W}	Nonrandomness factor. (Ratio of \mathbf{W}_E to \mathbf{g}_E).
P_{ig}, P_{vg}	Probably of viewing the understorey.
P_T, P_G	Proportion of sunlit canopy and sunlit understorey respectively.
P_{Tf}	Probability of viewing illuminated foliage when the view and illumination perspectives are not correlated.
P_{ii}	Proportion of observed tree crown that is illuminated
Q_1, Q_2	Probability of observing illuminated foliage elements with a tree crown.
R_G, R_T	Mean reflectance factor of the sunlit understorey, sunlit crown, shaded understorey, and
R_{ZG}, R_{ZT}	shaded crown respectively.
\mathbf{f}_v	View Azimuth Angle (often given relative to the IAA).
\mathbf{q}_v	View Zenith Angle
\mathbf{x}	Angle difference between the Sun and viewer. (scattering angle)
Z_T, Z_G	Proportion of shaded crown and shaded understorey respectively.
ZWH	Zenithal width of the hot spot

Table (1)

	OBS	OJP	YJP
Site Parameters			
Density	4000 tree/ha	1850 tree/ha	4000 tree/ha
Grouping	3	3	3
Quadrat Size	500 m ²	500 m ²	500 m ²
Crown Geometry			
a	130	220	300
H _c	1.9m	3.2m	1.5m
H _b	6.5m	4.0m	2.5m
H _a	0.5m	7.0m	0.5m
r	0.45m	1.30m	0.85m
Foliage Distribution			
G(θ)	0.5	0.5	0.5
LAI	4.5	2.2	2.7
Ω _E *	0.8	0.77	0.83
γ _E *	1.44	1.51	1.38
Reflectance Properties			
R _t (Red)	0.11	0.07	0.05
R _g (Red)	0.04	0.09	0.05
C _m F _{dt} (Red)	0.027	0.042	0.1
C _m F _{dg} (Red)	0.05	0.03	0.08
R _T (NIR)	0.5	0.53	0.53
R _G (NIR)	0.25	0.17	0.15
C _m F _{dT} (NIR)	0.2	0.25	0.36
C _m F _{dG} (NIR)	0.44	0.53	0.53

As published by Leblanc et al. [1998].

*Adapted from Chen [1996].

Table (2)

summer		OBS		YJP		OJP	
q_i	r_{cc} RMSE	(red)	(nir)	(red)	(nir)	(red)	(nir)
-15 ⁰	forward-FLAIR	.977 .006	.979 .026	.986 .003	.953 .014	.994 .003	.990 .015
	inverse-FLAIR (multi- q_i)	.986 .003	.990 .013	.992 .001	.911 .015	.997 .001	.993 .005
	inverse-FLAIR (uni- q_i)	.986 .003	.989 .010	.992 .002	.977 .010	.998 .001	.997 .004
-45 ⁰	forward-FLAIR	.979 .005	.979 .020	.970 .003	.949 .022	.984 .004	.977 .017
	inverse-FLAIR (multi- q_i)	.947 .007	.965 .024	.963 .003	.946 .019	.986 .003	.975 .012
	inverse-FLAIR (uni- q_i)	.993 .004	.993 .012	.980 .003	.970 .020	.991 .003	.993 .009
-75 ⁰	forward-FLAIR	.937 .009	.936 .032	.950 .003	.962 .025	.939 .006	.949 .032
	inverse-FLAIR (multi- q_i)	.937 .010	.935 .028	.938 .004	.972 .020	.942 .005	.956 .024
	inverse-FLAIR (uni- q_i)	.971 .002	.971 .008	.979 .002	.979 .010	.992 .001	.991 .005

Table (3)

Summer multi- q_i	OBS		YJP		OJP	
	Four-Scale	FLAIR	Four-Scale	FLAIR	Four-Scale	FLAIR
Red NIR						
LAI	4.5	2.6 3.0	2.7	2.7 2.7	2.2	2.4 2.4
R_{zt}	0.003 0.10	0.009 0.15	0.005 0.19	0.002 0.21	0.003 0.13	0.005 0.13
R_{zg}	0.002 0.11	0.000 0.08	0.004 0.08	0.002 0.09	0.003 0.09	0.002 0.08
R_t	0.110 0.50	0.055 0.32	0.050 0.53	0.053 0.57	0.070 0.53	0.039 0.39
R_g	0.040 0.25	0.073 0.36	0.050 0.15	0.046 0.17	0.090 0.17	0.110 0.22

(* Not calculated with the Four-Scale Model but using the approximation as outlined in the text.)

(Wavelength dependent values presented as Red | NIR where necessary)

Table (4)

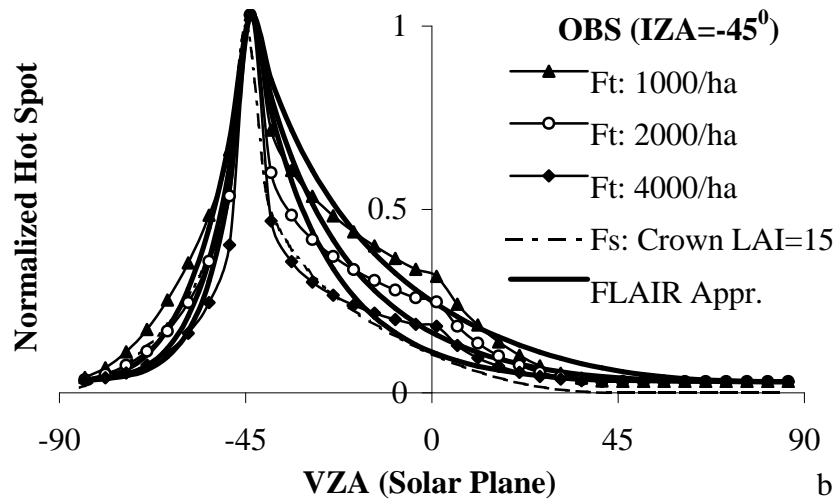
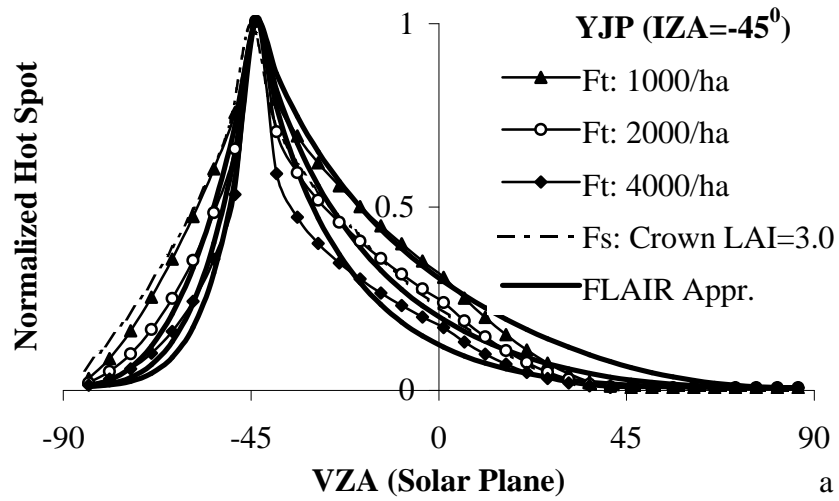


Figure (1)

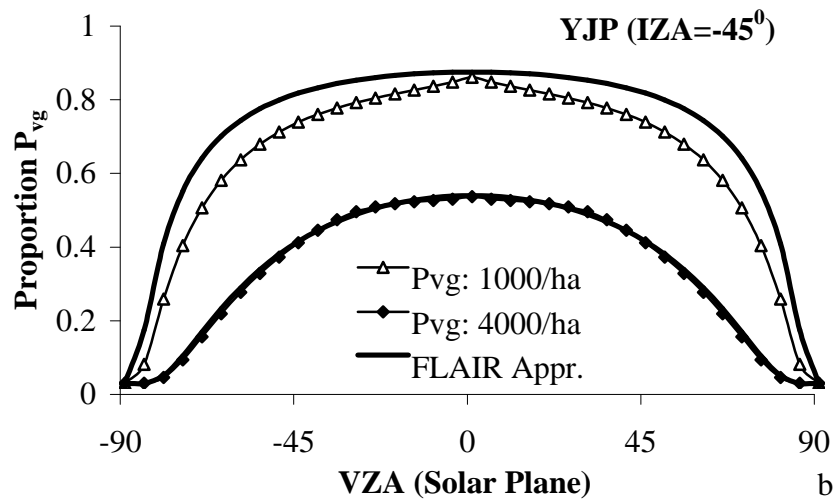
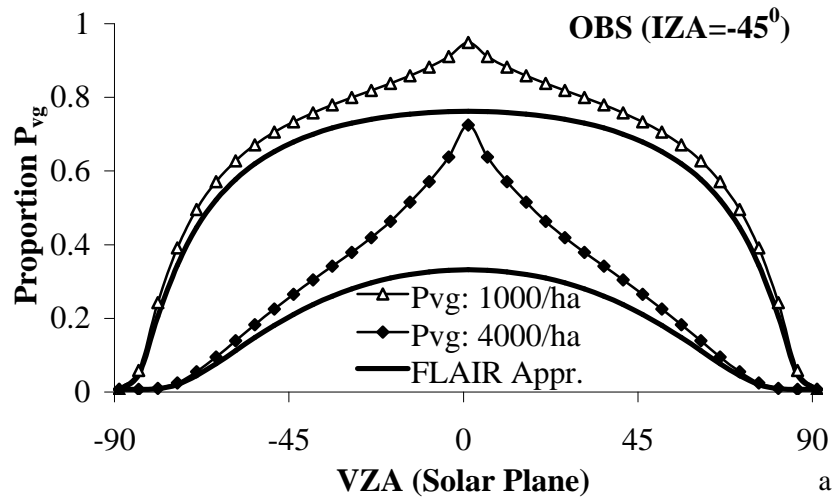


Figure (2)

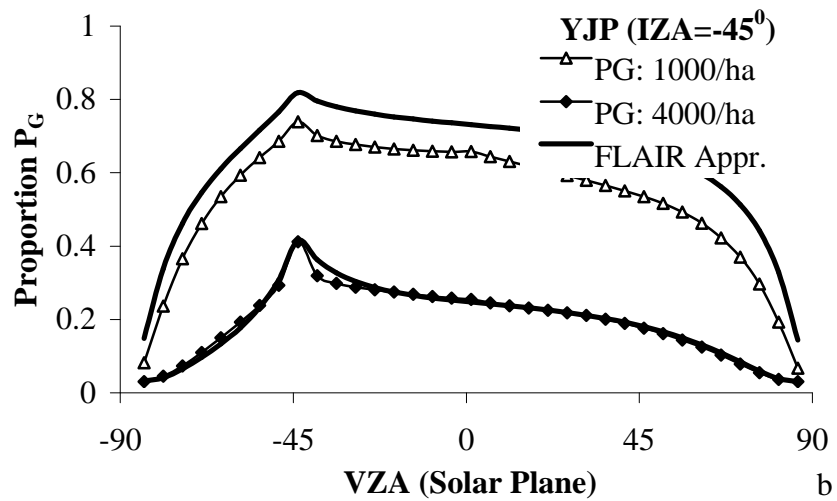
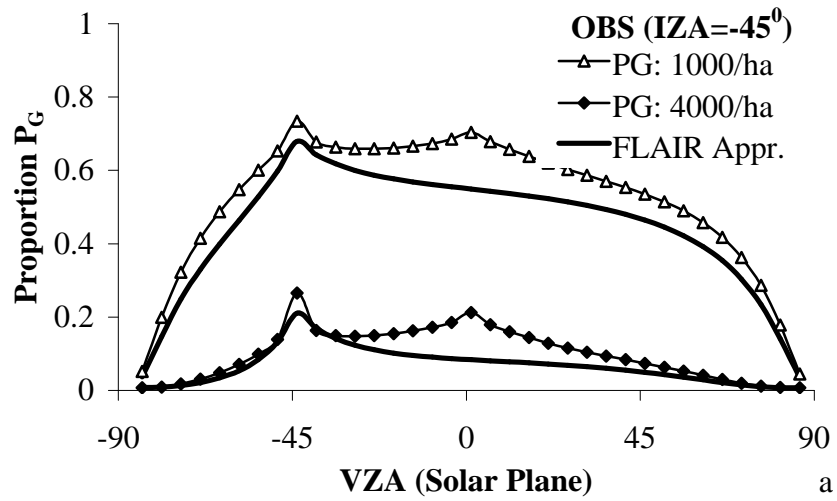


Figure (3)

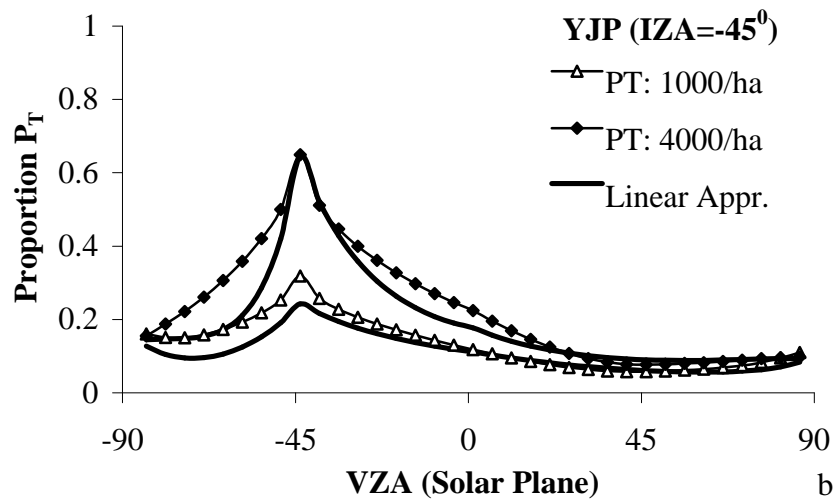
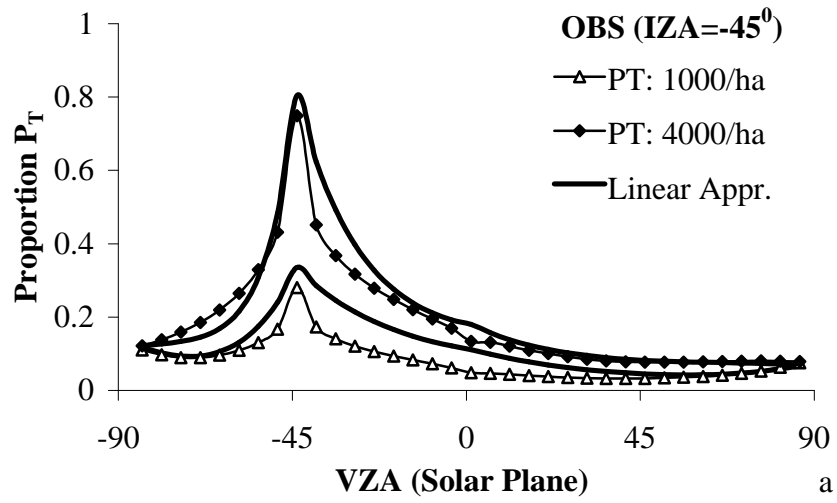


Figure (4)

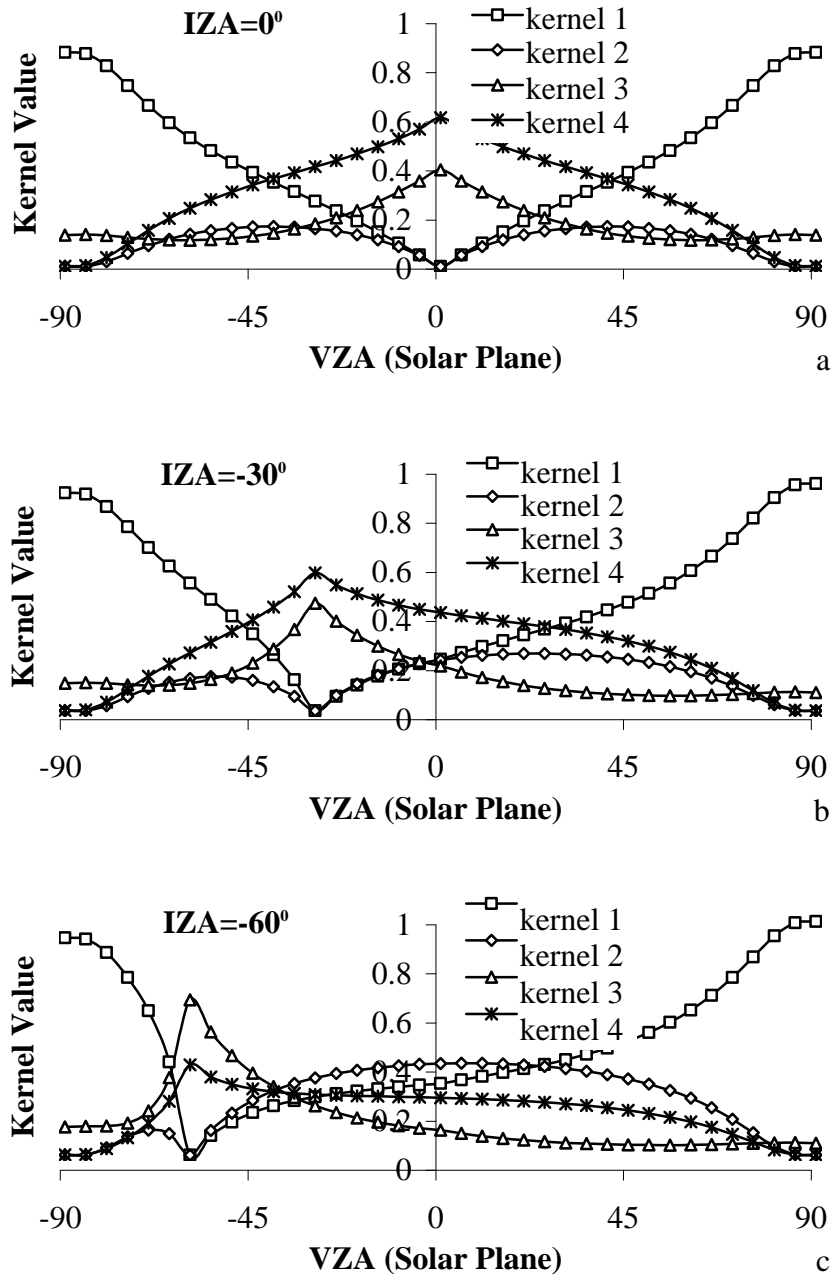


Figure (5)

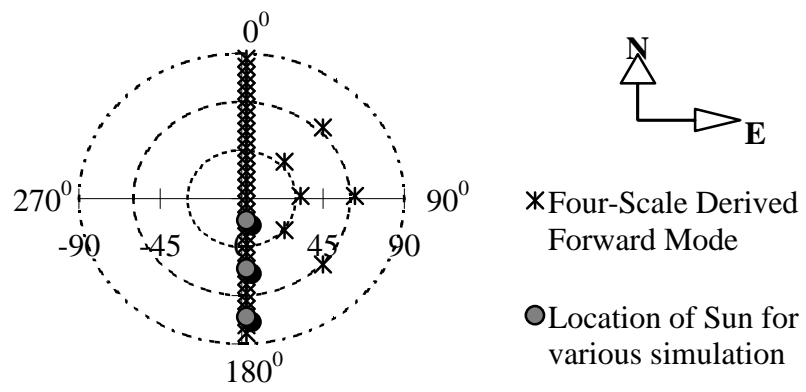


Figure (6)

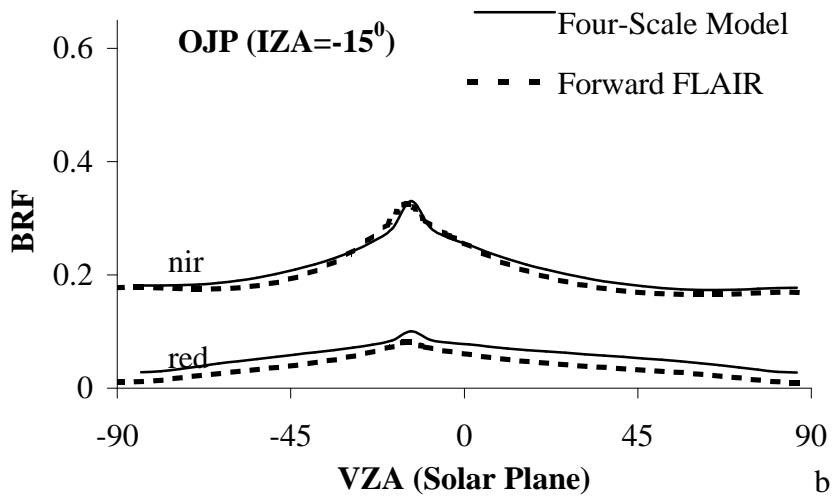
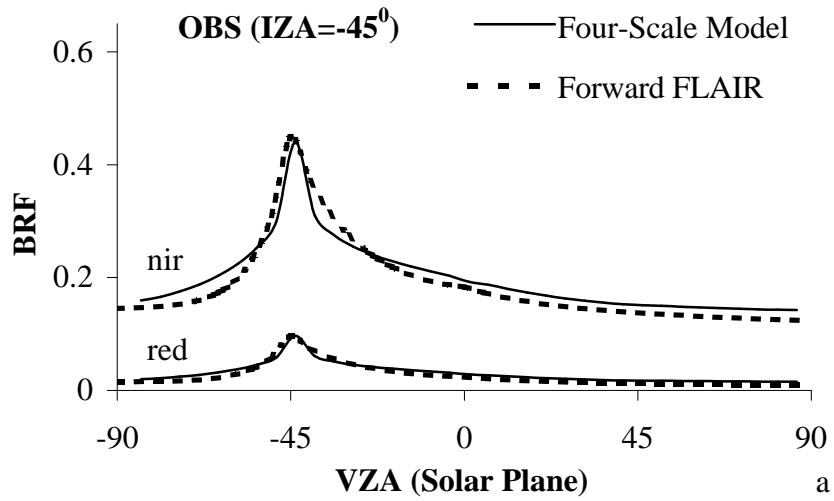


Figure (7)

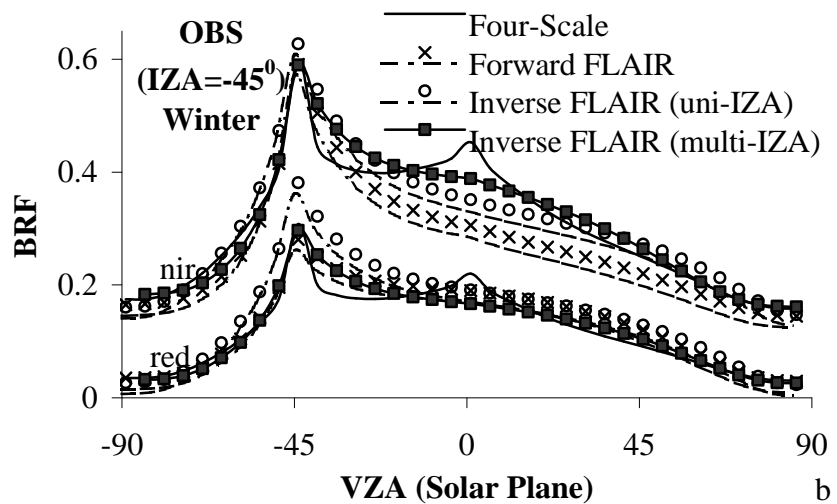
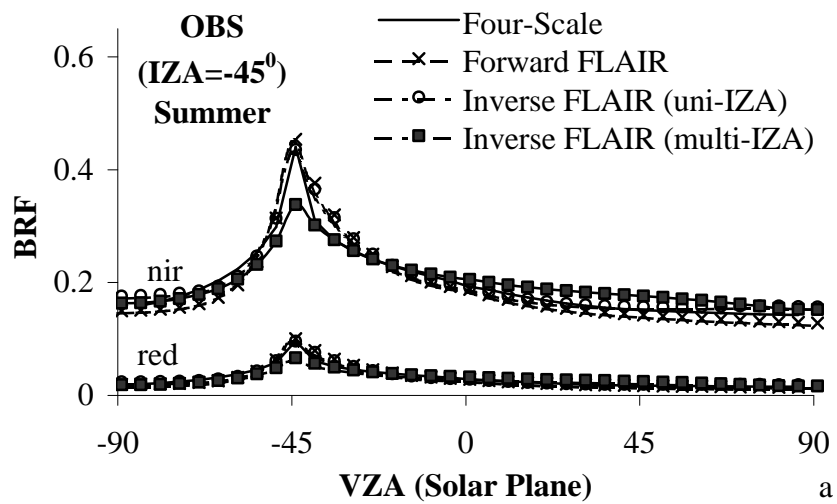


Figure (8)

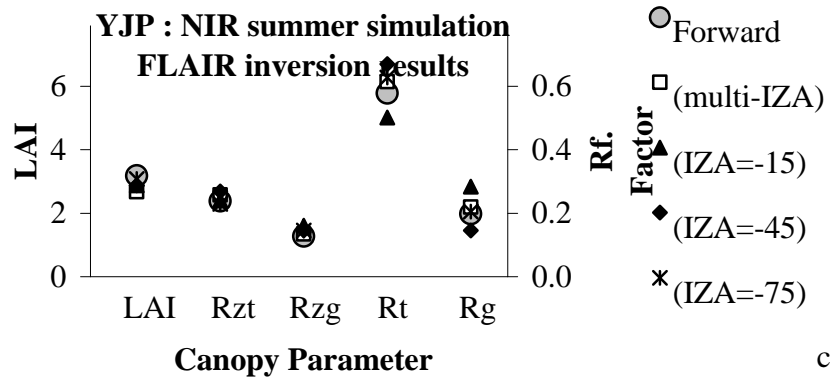
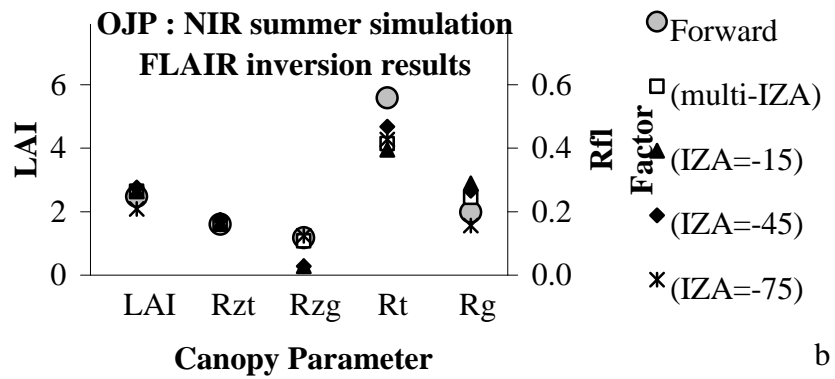
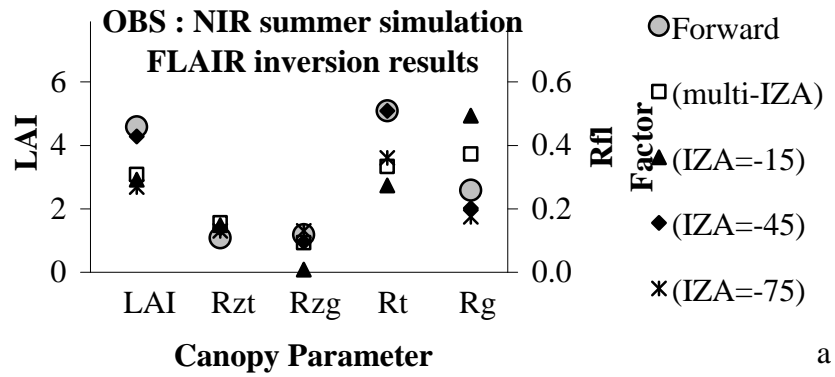


Figure (9)



H. Peter White received his B.Sc. degree in Physics and Astronomy from Saint Mary's University in 1988 and his M.Sc. (1994) and Ph.D. (1999) in Physics and Astronomy from York University.

He is currently a Canadian Government Laboratory Visiting Fellow at the Canadian Centre for Remote Sensing (CCRS) in Ottawa, Ont. His remote sensing interests have included Jovian planetary atmospheric composition and modelling optical bidirectional reflectance of boreal ecosystems. Current research is focused on modelling and retrieval of biophysical parameters of vegetative surfaces using optical remote sensing techniques.



John R. Miller received a B.E. degree (Physics) from the University of Saskatchewan, Saskatoon, in 1963, and both M.S.c. (1966) and Ph.D. (1969) degrees in space physics from the same university, studying the aurora borealis using rocket-borne radiometers.

He then spent two years on a postdoctoral fellowship at the Herzberg Institute at the National Research Council in Ottawa. In 1971 he went to work as a Project Scientist at York University. He is currently Professor of Physics and Astronomy at York University and is Co-director of the Earth Observations Laboratory of the Centre for Research in Earth and Space Technology (CRESTech). His remote sensing interests include atmospheric correction and interpretation of water colour reflectance and canopy reflectance. Over the past decade his primary focus has been on the application of reflectance spectroscopic techniques in remote sensing using imaging spectrometers.



Jing M. Chen received a B.Sc. degree in 1982 from Nanjing Institute of Meteorology, China, and a Ph.D. degree in 1986 from the University of Reading, Reading, UK.

He is currently a Research Scientist at the Canadian Centre for Remote Sensing (CCRS) in Ottawa, Ont., and a Professor in the Department of Geography, University of Toronto, Ont. His main research interests have been in turbulent and radiative transfer processes associated with plant canopies. He is currently engaged in research on applications of optical and microwave remote sensing techniques to boreal ecosystems. Research topics include radiation modelling, biophysical parameter retrieval, and modelling net primary productivity and carbon cycle.